# Vegetation Sensing Using GPS-Interferometric Reflectometry: Theoretical Effects of Canopy Parameters on Signal-to-Noise Ratio Data

Clara C. Chew, Eric E. Small, Kristine M. Larson, and Valery U. Zavorotny, *Fellow, IEEE*

***Abstract*—The potential to use GPS signal-to-noise ratio (SNR) data to estimate changes in vegetation surrounding a ground-based antenna is evaluated. A 1-D plane-stratified model that simulates the response of GPS SNR data to changes in both soil moisture and vegetation is presented. The model is validated against observations of SNR data from four field sites with varying vegetation cover. Validation shows that the average correlation between modeled and observed SNR data is higher than the average correlation between concurrent SNR observations from different satellite tracks at a site. The model also reproduces variations in the SNR metrics amplitude, phase, and effective reflector height over a range of vegetation wet weights from 0 to 4 kg · m$^{-2}$, with $r^2$ values of 0.79, 0.84, and 0.62, respectively. Model simulations indicate that the amplitude of SNR oscillations may be used to estimate vegetation amount when vegetation wet weight is below 1.5 kg · m$^{-2}$. When vegetation wet weight exceeds 1.5 kg · m$^{-2}$, the sensitivity of amplitude to changes in vegetation amount decreases. Phase of SNR oscillations also varies consistently with vegetation up to 1.5 kg · m$^{-2}$. However, phase is also very sensitive to soil moisture variations, thus limiting its utility for estimating vegetation. Effective reflector height is not a consistent indicator of vegetation change. Beyond 1.5 kg · m$^{-2}$, the constant frequency assumption used to characterize SNR fluctuations does not adequately describe observed data. A more complex approach than the standard SNR metrics used here is required to extend GPS-Interferometric Reflectometry sensing to thicker canopies.**

***Index Terms*—Global Positioning System, radar, reflectometry, remote sensing.**

## I. Introduction

QUANTIFYING key vegetation parameters, including the timing and duration of green-up, maturity, senescence, and dormancy, is important for phenologists, climate scientists, and agriculturalists [1]. These parameters are essential in understanding the effect of shifting precipitation regimes on ecosystems, ensuring future food security, and in the implementation of variable-rate technologies such as fertilizer applications [2], [3]. In addition, quantifying vegetation extent, such as vegetation water content, is important to soil scientists interested in using remote sensing data products for soil moisture estimation. This is because soil moisture estimations are affected by changes in vegetation cover [4], [5]. The constellation of GPS satellites (microwave-transmitting antennas) together with ground-, plane-, or space-based receiving antennas can be used to sense environmental variables in a bistatic radar approach. Numerous investigators have employed this general technique to study the ocean and land surface [6]. Ocean studies have focused on surface height and wind speed retrieval, and both theoretical [7] and experimental studies [8] have proven the utility of the approach, even for receiving antennas that are stationed in low earth orbit [9]. Terrestrial properties may also be estimated using bistatic sensing of reflected GPS signals (e.g., [10] and [11]). A subset of these studies has been focused on vegetation. Most of these studies have used antennas or receivers specifically designed for the task [12], [13]. It was suggested in [14] that geodetic-quality antennas/receivers could be used for vegetation sensing. This technique, known as GPS-Interferometric Reflectometry (GPS-IR), is attractive because ground-based GPS networks already exist that can provide data for vegetation studies.

GPS-IR utilizes GPS antennas and receivers that are normally used for tectonic or surveying applications to retrieve environmental conditions over an area of approximately 1000 m$^2$ around the antenna [15]. This technique is different from other bistatic reflectometry methods in that it does not require a specially designed antenna or receiver in order to estimate environmental parameters (e.g., [13] and [16]). This technique is currently used at many of the already existing GPS stations that comprise NSF's EarthScope Plate Boundary Observatory (PBO) network to estimate changes in snow depth [17].

GPS-IR takes advantage of the interference of the coherent direct and reflected GPS signals [Fig. 1(a)], which is recorded in signal-to-noise ratio (SNR) interferograms. For a typical geodetic-quality GPS antenna's gain pattern, this interference is greatest at satellite elevation angles smaller than 30° (90° being defined as zenith), as shown in Fig. 2(a). For environmental sensing, the SNR data are converted to a linear scale and detrended with a low-order polynomial to remove the effect of the direct signal [15]. The detrended portion, which oscillates around zero, is shown in Fig. 2(b). In this paper, we will use the term SNR to mean the detrended portion of the signal.

Manuscript received August 12, 2013; revised November 18, 2013, May 15, 2014, and July 31, 2014; accepted September 25, 2014. This work was supported in part by National Science Foundation under Grant AGS-0935725 and the National Aeronautics and Space Administration under Grant NNX12AK21G and NNX13AF43G.

C. C. Chew and E. E. Small are with the Department of Geological Sciences, University of Colorado, Boulder, CO 80309-0399 USA (e-mail: clara.chew@colorado.edu; eric.small@colorado.edu).

K. M. Larson is with the Department of Aerospace Engineering Sciences, University of Colorado, Boulder, CO 80309 USA (e-mail: kristinem.larson@gmail.com).

V. U. Zavorotny is with the Earth Systems Research Laboratory, National Oceanic and Atmospheric Administration, Boulder, CO 80305-3337 USA (e-mail: valery.zavorotny@noaa.gov).

Color versions of one or more of the figures in this paper are available online at http://ieeexplore.ieee.org.

Digital Object Identifier 10.1109/TGRS.2014.2364513

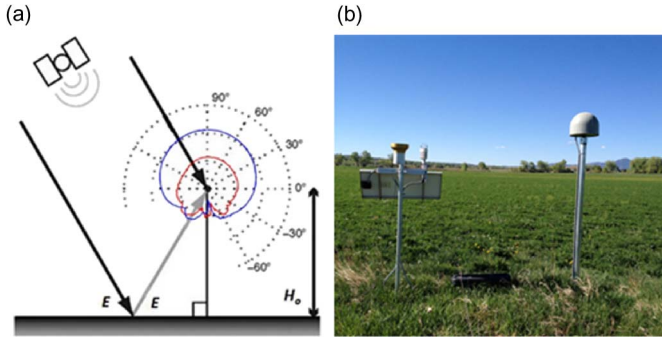


Fig. 1. (a) Geometry of a multipath signal, for antenna height $(H_o)$ and satellite elevation angle $(E)$. Bold black lines represent the direct signal transmitted from the satellite. The gray line is the reflected signal from the ground. The antenna's phase center is shown as the small dot. The blue line/outer ring (higher gain) represents the RHCP gain of the antenna. The red line/inner ring (lower gain) represents the LHCP gain of the antenna. At 0°, the RHCP and LHCP gains are approximately −38 and −50 dB, respectively. At 90°, the RHCP and LHCP gains are approximately −20 and −40 dB, respectively. (b) Photograph from the alfalfa field in Colorado, showing the GPS antenna, receiver box, and solar panel typical of all field sites in this study.

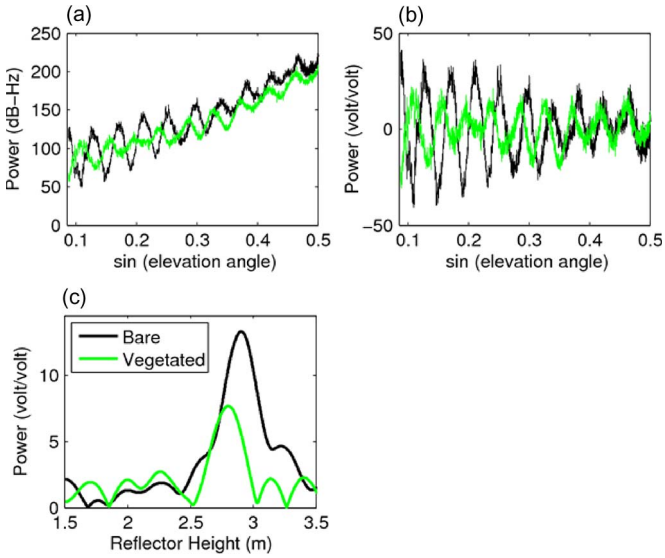


Fig. 2. Black lines indicate data retrieved when ground was bare. Green lines indicate data retrieved when ground had 2.5 kg · m$^{-2}$ of vegetation present. Data are from the soybean site. (a) SNR data from one satellite on two separate days. Data still have the direct component. (b) Same SNR data as from panel (a) but with the direct component removed and transformed to a linear scale. (c) LSPs indicating the frequency content of SNR curves in panel (b).

Detrended SNR data have previously been modeled using the following equation [18]:

$$\text{SNR} = A\cos\left(\frac{4\pi H_0}{\lambda}\sin E + \phi\right) \tag{1}$$

where $H_0$ is the height of the antenna, $E$ is the elevation angle of the satellite, $A$ is a constant amplitude, $\lambda$ is the GPS wavelength (∼24.4 cm), and $\phi$ is a phase shift. This expression assumes that the SNR data have a constant frequency $(4\pi H_0/\lambda)$. The observations in Fig. 2(b) show that $A$ is not constant but depends upon elevation angle. However, we use this approximation to minimize the number of parameters required to describe the SNR curve. The simplified, constant frequency, and constant amplitude expression does not significantly affect bare ground soil moisture estimations [19]. One goal of this paper is to assess if these simplifications are also valid for vegetation sensing. $A$ and $\phi$ are found from the SNR data using least-squares estimation, with $H_0$ set to the best approximation of the height of the antenna. In practice, the actual antenna height is not the same for all satellite tracks due to variations in surface elevation surrounding the antenna. For observed data, $H_0$ is derived empirically using the temporal average of bare soil or minimal vegetation values of effective reflector height. This average is referred to as the "*a priori* reflector height," and it varies between satellite tracks. The procedure to estimate the *a priori* reflector height and effective reflector heights is described in the following discussion.

It has been shown both in field experiments and a modeling study that $A$ and $\phi$ are sensitive to changes in soil moisture content for a bare soil [19], [20]. This is because the ground surface's permittivity or dielectric constant is primarily a function of its water content, for microwave frequencies. The permittivity of the reflecting surface determines the characteristics of the reflected signal, which affects the SNR interferogram.

Other studies have explored how the frequency of the SNR interference pattern changes in response to changes in snow depth [17] and water level [21], [22]. In these cases, a Lomb-Scargle periodogram (LSP) is used to estimate the dominant frequency of the SNR curve [two examples of LSPs are shown in Fig. 2(c)] [23]. An LSP is like a Fourier transform, except that it is able to analyze the unevenly sampled data that are recorded by the GPS receiver. This method of data analysis is not used in the estimation of phase or amplitude described previously in (1), except to choose the *a priori* reflector height $H_0$. The peak frequency of the LSP is converted into an effective reflector height $H_{\text{eff}}$ using the following equation [24]:

$$H_{\text{eff}} = \frac{1}{2} f_m \lambda \tag{2}$$

where $f_m$ is the peak frequency of the LSP. Note that $H_{\text{eff}}$ may differ greatly from the *a priori* reflector height $H_0$ in (1). For sea and snow level studies, $H_{\text{eff}}$ varies through time as the reflector distance changes. This is due to the fact that the permittivity of water (and frequently for snow) is high enough so that the surface of the water or snow acts as a single reflector for the multipath signal, with minimal influence from the underlying medium. In contrast, for soil moisture studies, $H_{\text{eff}}$ typically only varies by several centimeters around $H_0$.

Here, we use field data and an electrodynamic forward model developed in [25] to quantify how changes in vegetation affect SNR metrics (phase, amplitude, and effective reflector height) for different plant canopies. This model was used in [19] to illustrate the effect of changes in soil moisture on SNR metrics for a bare soil. In this paper, we adapt the model by adding a layer of homogeneous vegetation on top of the soil. We also examine how vertical variations in the vegetation canopy affect metrics. First, we describe our model and validate it against field observations. Validation occurs in two steps. First, we quantify the correlation between observed and modeled SNR curves across a range of vegetation wet weights. Second, we assess how well the metrics calculated from the modeled SNR data reproduce the corresponding metrics determined

from observed SNR data. Next, we use the model to quantify how SNR metrics should theoretically respond to changes in vegetation characteristics, specifically changes in vegetation wet weight, which is the amount of vegetation covering the ground in kilograms per square meter. This provides guidance for knowing when and where SNR-based metrics can be used for vegetation retrievals.

## II. Forward Model Description

### A. Vegetation Model

The 1-D electrodynamic single-scattering forward model that we adapted to simulate SNR data in this study was developed in [25] and further explored in [19]. The model was originally developed for bare soil simulations for a flat surface surrounding an antenna. It requires user-defined point soil moisture estimates at specified depths within the soil column. A piecewise cubic interpolation between depths is used to produce a soil moisture profile that is 20 cm thick, discretized into 1-mm layers, each with its own soil moisture value [19]. In this paper, however, we assume a soil column with uniform soil moisture at all depths. This simplification is justified as [19] found that soil moisture variations with depth only minimally impacted SNR metrics.

Soil moisture values are converted into complex permittivity values, using relationships in [26]. These relationships were derived for volumetric soil moisture and permittivity at L-band frequency for five different soil types using a semiempirical model [26]. Here, we only report results for a loam soil, as [19] showed that soil type has a negligible impact on SNR metrics.

Our adapted model uses specified vegetation canopy parameters and produces a 1-D homogenous permittivity profile of the plant canopy on top of the soil. There is an abrupt contrast between the canopy top and the air above the canopy. A plane-stratified model for vegetation was also used in [27], and it was found that such an abrupt transition between the top of the canopy and air could create constructive and destructive interference that is not observed in field data. In Section III, we will provide an example of how a less abrupt, or gradual, canopy top affects the simulation of SNR data.

Many studies have used plane-stratified models to simulate emission from vegetation canopies at microwave frequencies (e.g., [27] and [28]). This is in contrast to a geometrical modeling approach, in which each component of the plant canopy, such as stalks and leaves, is modeled by their geometrical shapes (e.g., [29] and [30]). Geometrical modeling is used because, at microwave frequencies, a canopy layer is often considered inhomogeneous and anisotropic [31]. Geometric effects are most important when the components of the canopy, i.e., stalks, leaves, or branches, are the same size or larger than the wavelength of the signal. Because the wavelength of the GPS L-band signal is $\sim$24 cm, which is much longer than X- or C-bands ($\sim$3 and 5 cm, respectively), we use a plane-stratified model that does not consider internal canopy geometry. Geometric models, which would take into account the relative distribution and orientation of stalks of leaves, are commonly used in radar remote sensing and would likely lead to better agreement with observations. We decided on a plane-stratified approach due to its ability to use only commonly measured field parameters as input, with no additional information needed about individual plant components. For the range of vegetation types that we tested in this study, geometric components of the canopy were smaller than the wavelength of the L-band signal. Our validation results demonstrate that the plane-stratified model is sufficient for the canopies studied here. However, our model might not accurately simulate vegetation types that have geometric components of greater than 24 cm.

Assuming that structural geometric effects are negligible means that we neglect the coherence loss of the reflected wave due to volume scattering within the plant canopy due to geometric effects. However, our model does take into account multiple reflections between 1-D layers within the medium if they exist, which does allow for modeling the resulting coherence loss from permittivity changes.

At its most basic level, the model uses volumetric soil moisture estimates at specified depths within the soil column and specific vegetation canopy parameters as input to produce theoretical SNR curves. We split our explanation of the model into two general parts: permittivity profile generation and estimation of reflected power received at the antenna.

*Permittivity Profile Generation:* For reasons described in the following section, it is necessary for the model to convert the soil moisture depth measurements and vegetation canopy parameters into a 1-D stratified permittivity profile. Creation of the permittivity profile for the soil layers was described previously.

Vegetation input parameters include vegetation wet weight (in kilograms per square meter), dry biomass (in kilograms per square meter), canopy height (in meters), vegetation water salinity (in per mill), and vegetation plant matter density (in kilograms per cubic meter). The height of the vegetation permittivity layer is thus canopy height. All of these parameters, except salinity, were based on extensive vegetation surveys at four field sites. The way we used these field measurements is described in the following discussion.

The permittivity of the vegetation is estimated using a model developed in [32], which requires the frequency (L-band), salinity of vegetation water, and vegetation water content (which we derived from wet weights and dry biomasses) to produce a complex permittivity of the vegetation matter. The model in [32] was developed using field measurements of corn leaves but found good agreement when the model was extended to different vegetation types. We use their average value of vegetation water salinity for all of our model simulations.

Because the vegetation canopy is actually a mixture of plant matter and air, we use the Complex Refractive Index mixture equation from [33] to get the resulting permittivity of the canopy

$$\varepsilon_{\mathrm{canopy}}^{1/2} = v_{\mathrm{veg}}\varepsilon_{\mathrm{veg}}^{1/2} + v_{\mathrm{air}}\varepsilon_{\mathrm{air}}^{1/2} \tag{3}$$

where $v_{\mathrm{veg}}$ is the volume fraction of vegetation in the canopy, $v_{\mathrm{air}}$ is the volume fraction of air in the canopy, $\varepsilon_{\mathrm{veg}}$ is the permittivity of vegetation, and $\varepsilon_{\mathrm{air}}$ is the permittivity of air (1.0).

TABLE I
GPS STATIONS, ANTENNA HEIGHTS, AND VEGETATION PARAMETERS

| Station | Antenna height (m) | Years with data | # of validation surveys | Range of Data | | | Mean Calculated Permittivity |
|---|---|---|---|---|---|---|---|
| | | | | Wet weight (kg m-2) | Canopy height (cm) | Dry biomass (kg m-2) | |
| Desert Steppe A | 1.96 +/-0.03 | 2011 | 21 | 0.16-0.71 | 8-47 | 0.1-0.35 | 1.03+0.009i |
| Desert Steppe B | 2.83 +/-0.03 | 2012-2013 | 39 | 0.08-.32 | 3-31 | 0.03-0.24 | 1.015+0.005i |
| Rangeland C | 2.72 +/-0.06 | 2011-2012 | 29 | 0.29-1.02 | 5-38 | 0.19-0.65 | 1.03+0.011i |
| Rangeland D | 2.82 +/- 0.03 | 2011-2012 | 30 | 0.33-1.55 | 3-49 | 0.20-1.01 | 1.035+0.011i |
| Rangeland E | 3 +/- 0.05 | 2011-2012 | 30 | 0.36-1.44 | 8-32 | 0.23-0.98 | 1.04+0.017i |
| Alfalfa | 2.69 +/- 0.15 | 2011-2013 | 56 | 0.11-4.95 | 5-80 | 0.06-2.59 | 1.06+0.013i |
| Soybean | 2.96 +/- 0.09 | 2012 | 5 | 0.04-2.57 | 9-90 | 0.01-0.78 | 1.04+0.004i |

The volume fractions of air and vegetation are estimated by knowing the canopy height, assuming a universal dry bulk density of vegetation (300 $\mathrm{kg} \cdot \mathrm{m}^{-2}$, the average from laboratory experiments), and assuming that the density of plant matter above its bulk value is proportional to its percent water content. The effective permittivity of the canopy is often very close to that of air, which is expected, given that most plant canopies are comprised mostly of air [34]. Our calculated values agree well with published values using time domain reflectometry to measure canopy permittivity, which are also very close to the permittivity of air (Table I) [35].

*Estimation of Reflected Power Received at the Antenna:* After the combined soil/vegetation permittivity profile is generated, the model estimates both right- and left-handed reflection coefficients that would result from a GPS multipath signal reflecting out of the soil/vegetation layers at a specified angle of incidence (elevation angle). The reflection coefficients are combined with the left- and right-handed values of the antenna gain at that elevation angle to get the resulting power of the reflected signal. Altering the gain pattern will alter the reflected power. The model uses values of gain for a GPS choke ring antenna typical of our field sites measured in an anechoic chamber.

The procedure described previously is repeated for each specified elevation angle in the user-specified range. In this paper, we use an elevation angle range of 5°–30°, in approximately 0.002° increments, which is the range used in previous GPS-IR studies [20], [36]. The interference between the power of the direct and indirect signals makes up the modeled SNR data. A more detailed explanation of model mechanics is described in [25], and it will not be included here.

## III. MODEL VALIDATION

The purpose of model validation is to evaluate if the model can successfully simulate SNR data observed in the field. This validation is completed across a range of vegetation canopies. We first compare the modeled and observed SNR curves, calculating how the correlation between modeled and observed data varies with vegetation water content. Then, we test whether the model can reproduce observed SNR metrics (phase, amplitude, and effective reflector height) and how they vary with vegetation parameters. In this section, we describe what field data we use for validation, how we define successful validation, and our results.

### A. Validation Setup: Field Observations and Model Input

For model validation, we use observed SNR data from GPS antennas situated among four different vegetation types: managed alfalfa [Fig. 1(b)], cultivated soybeans, grazed rangeland, and desert steppe. The GPS systems at these sites have identical hardware (Trimble NetRS receivers and Choke-Ring antennas with a radome), although the height of each antenna varies slightly. Some of the field sites have multiple antennas operating concurrently and/or located closely to one another; this information is summarized in Table I.

Each of the antennas is also instrumented with Campbell Scientific 616 soil moisture probes (at least five probes at 2.5 cm depth, five at 7.5 cm, and two at 20 cm). The soil moisture probes each record data every 30 min, although we average the data from the probes to get one daily value at each depth. Vegetation samples were collected regularly throughout the growing season (see Table I for vegetation statistics). An individual vegetation sampling survey consists of collecting seven vegetation samples, at random azimuths and distances (between 7 and 35 m), around an antenna. At each sampling location, a 30 × 30 cm grid is tossed on the ground, vegetation canopy height is measured, and all vegetation within the grid is cut and weighed. The cut vegetation is then dried for 48 h at 50 °C and weighed again, to measure how much water was in each sample. The dried vegetation is the dry biomass. Once the information from the seven samples is averaged, we have estimates of the mean canopy height, water content, and dry biomass on each day that samples were collected. This vegetation collection does not modify site characteristics to any noticeable degree, given the relatively larger sensing area of each antenna. For example, 15 sampling days during a growing season would disturb only 10 $\mathrm{m}^2$ of vegetation, about 1% of the sensing area within the GPS footprint.

We use the mean field vegetation and soil moisture data as the inputs to our model. Thus, each sampling day has one corresponding SNR curve generated from the mean vegetation and soil moisture data collected on that day.

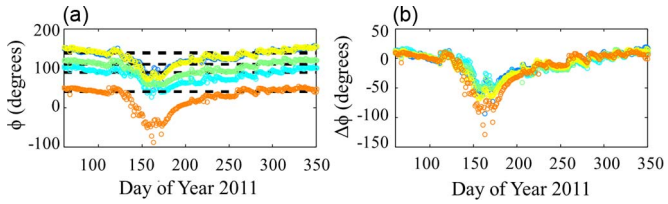


Fig. 3. (a) Observed phase time series for five satellite tracks at the Rangeland C antenna (colored dots). Dashed lines indicate the estimated baseline phase value for each satellite track. (b) Observed phase time series values after the baseline phase has been removed.

We use observed SNR data from five satellite tracks at most sites, although we only use two and three tracks from antennas D and E at the rangeland site, respectively. Tracks were selected such that none was influenced by trees or had significant topography. Phase, amplitude, and effective reflector height are computed from the SNR data from each satellite track. $H_0$ for each satellite track was determined empirically using the procedure described previously.

Comparing observed SNR data across sites necessitated first rescaling each of the three metrics. For example, SNR amplitude is not only affected by soil moisture and vegetation but also by the satellite transmit power (which is different for each satellite) and, to a lesser extent, the temperature of the receiver [37]. It can also be affected by the cable between the antenna and receiver. This means that the largest amplitude at the soybean site is different than the largest amplitude at the rangeland site for technical reasons, not because the soil moisture or vegetation conditions differ. To mitigate this issue, we normalized amplitude for each site by dividing each daily-mean amplitude value by the maximum daily-mean amplitude observed at that site. Thus, each site's normalized amplitudes range from 0 to 1, instead of having a maximum of 18 or 16 V/V, etc. We report these values as $A_{\mathrm{norm}}$. Because the height of the GPS antenna is different for every site, we only looked at $H_{\mathrm{eff}}$ deviations from $H_0$ $(\Delta H_{\mathrm{eff}})$.

At a field site, the observed daily variations in phase from two different satellite tracks may be very similar, even though the baseline phase value for the satellite tracks may be very different. Fig. 3(a) shows the phase time series for different satellites at the rangeland site. All exhibit a substantial decrease in phase during the summer, as well as smaller magnitude variations throughout the year. However, satellites differ in their baseline phase values. This is because the elevation angle at which the receiver initially locks onto the satellite is different, as well as differences in the value of $H_0$ that was estimated. Baseline phase differences present a challenge when trying to quantitatively compare the observed phase time series. In addition, this complicates comparisons to the modeled time series. Simulated phase does not depend on when the receiver locks onto a satellite but rather the arbitrary phase of the transmitted signal set at 5° elevation angle in the model. The difference in baseline phase is also an issue when comparing the entire observed or modeled SNR curves, since a small difference in phase will cause a low correlation between two curves, even if the shapes themselves match well.

To mitigate these issues, we subtract the satellite's baseline phase value from each observed time series to effectively "zero" the time series and get a change in phase from the baseline $(\Delta\phi)$ [Fig. 3(b)]. Baseline phase values represent the time during the year when there is the least amount of vegetation. The baseline value is selected to be the median phase value. For the four field sites, this occurs during times of the year when vegetation is either dormant or absent. We also zero our modeled phase values, although we cannot use exactly the same approach. There are relatively few modeled phase values in our time series because the model is only run for days when vegetation was sampled. Therefore, we choose the modeled baseline phase as the value that corresponds to the lowest observed vegetation wet weight. After zeroing the observed and modeled phase time series, both are approximately zero when there is little to no vegetation and are less than zero when vegetation grows.

### *B. Comparison of Simulated and Observed SNR Data*

The first goal of model validation is to evaluate if modeled SNR data match well with observed. As just described, comparing SNR data requires that one curve is shifted to account for offsets. Because of this, we performed a cross-correlation on the modeled and observed SNR curves to determine the phase lag that would allow for the highest correlation $(\gamma)$ between the two curves. This shifting is done on a track-by-track basis. The modeled data are thus shifted to best match the observed data. This means that, when we compare the shapes of modeled and observed SNR data, we are comparing their shape only and not how their respective phases change due to soil moisture or vegetation. The modeled and observed phase shifts are compared separately (Section III-C).

Two examples of observed and modeled SNR data from the soybean site are shown in Fig. 4(a) and (b). The observed SNR data are from one satellite track—different satellite tracks have slightly different SNR data. The modeled SNR curves for bare soil and vegetated conditions match the corresponding observed SNR curves. The model reproduces the reduction of amplitude resulting from the addition of vegetation. In addition, variations in amplitude with elevation angle that result from the presence of vegetation are also well simulated. The SNR data simulated using the gradual canopy top (meaning the permittivity was allowed to decrease to 1.0 over the top 10% of the canopy) do not match the observations as well as the SNR data simulated with the homogeneous canopy, although the differences between the two are small compared to the changes associated with adding a vegetation canopy.

The modeled and observed periodograms are similar [Fig. 4(c) and (d)], although the match is not as close as that for the SNR data. In particular, the maximum power of the periodogram is less in the observed data than modeled data, for both bare soil and vegetated conditions. This could be a result of colored noise in the observations, due to terrain effects in real environments, or differences in the modeled and observed satellite transmit power or antenna gain pattern.

In the bare soil example [Fig. 4(a)], $\gamma$ between the model simulation and observed SNR data is 0.87. For the example with vegetation, $\gamma$ between the observed SNR data and the simulation with the abrupt canopy top is 0.81, and $\gamma$ between

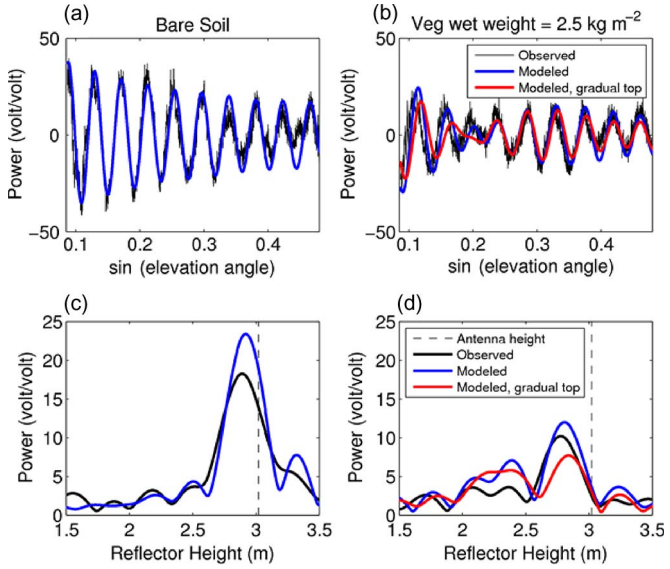


Fig. 4. (a) Black line is SNR data from one satellite passing over the soybean site when ground was bare. Blue line is one modeled representation with a soil moisture of 0.15, using field inputs from the same day as the observed data. (b) Same as in (a), except for when the vegetation was at its maximum extent (vegetation wet weight 2.5 kg $\cdot$ m$^{-2}$). The red line uses the same field inputs as the blue line, except also with a gradual canopy top that begins to thin out at 90% height. (c) Corresponding LSPs for the curves in (a). (d) Corresponding LSPs for the curves in (b).

TABLE II
MEAN CROSS-CORRELATION COEFFICIENTS

| Station | Mean $\gamma$ value | |
|---|---|---|
| | Model and Observations | Observations and other concurrent observations |
| Desert Steppe | 0.86 | 0.82 |
| Rangeland | 0.77 | 0.71 |
| Alfalfa | 0.72 | 0.65 |
| Soybeans | 0.72 | 0.65 |

the observed SNR data and the simulation with the gradual canopy top is 0.70. A $\gamma$ value of 1 would indicate a perfect match; however, because observed data contain noise, it will never be 1.

We computed $\gamma$ between our modeled and observed SNR data at our four field sites. For each day that vegetation was sampled at our sites, we chose observed SNR data for up to five different satellite tracks and computed $\gamma$ between the modeled SNR data and each satellite observation. We also computed $\gamma$ between observed SNR data from the different satellite tracks. This means that we computed $\gamma$ between the first satellite track and the second, $\gamma$ between the first satellite track and the third, $\gamma$ between the second satellite track and the third, and so on. Observed $\gamma$ values are useful because they indicate the differences that may occur in observed data—due to azimuthal differences in vegetation or soil moisture, differences in the amount of noise in the observed data, or differences in satellite transmit powers. At all four field sites, the average $\gamma$ value between the model and observations was higher than the value between concurrent observations (Table II). This indicates that the variability between data from individual satellite tracks is greater than the differences between observations and the modeled data. From this analysis, we conclude that our model is able to successfully simulate observed SNR data, at least relative to the natural variability that exists in observed data.

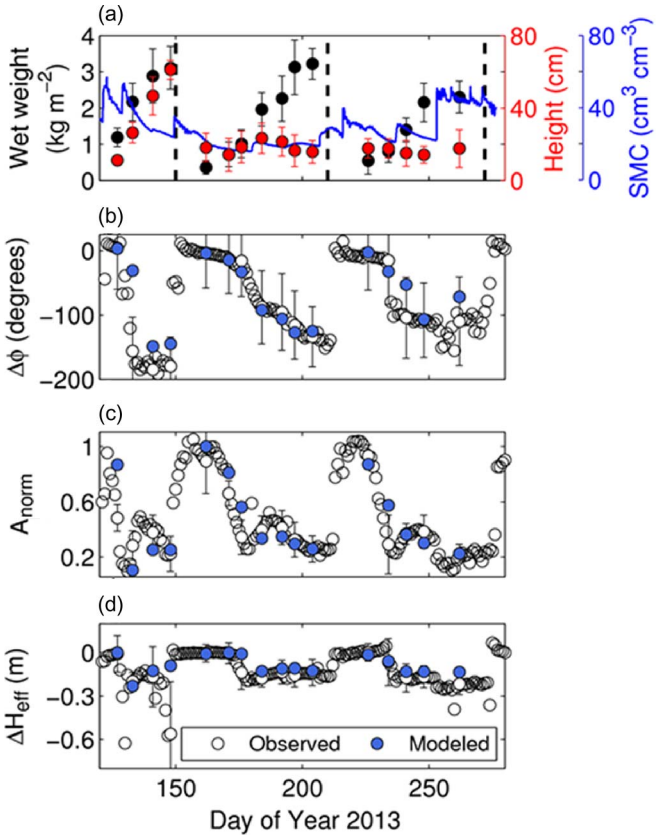


Fig. 5. (a) Field vegetation wet weight (black) and canopy height (red) for the alfalfa site in 2013. Error bars are the standard deviation of the seven collected field samples. Dashed lines indicate the approximate date of each harvest. (b)–(d) Time series of GPS metrics, both modeled and observed, at the alfalfa field site in 2013. Open white circles are the average metric observed from five satellite tracks. Error bars are the standard deviations of the metrics on each day when vegetation was sampled. Error bars are not shown on every day for clarity. Blue circles are the modeled metric, using average vegetation and soil moisture field data as input.

### C. Comparison of Simulated SNR Metrics and Observed Metrics

The second goal of model validation is to evaluate if modeled SNR metrics respond to changes in vegetation in the same way as observed SNR metrics. Example time series of observed and modeled SNR metrics for the alfalfa site from 2013 are shown in Fig. 5. In a qualitative sense, the model is able to reproduce the fluctuations in SNR phase, amplitude, and effective reflector height observed at this site. Vegetation field data [Fig. 5(a)] show that the alfalfa was harvested three times during 2013. The relationship between vegetation wet weight and canopy height changed substantially after the first harvest. The observed SNR data [Fig. 5(b)–(d)] mimic the three observed growth cycles. The value of each metric decreases as the alfalfa grows. Then, each metric returns to approximately the original value after

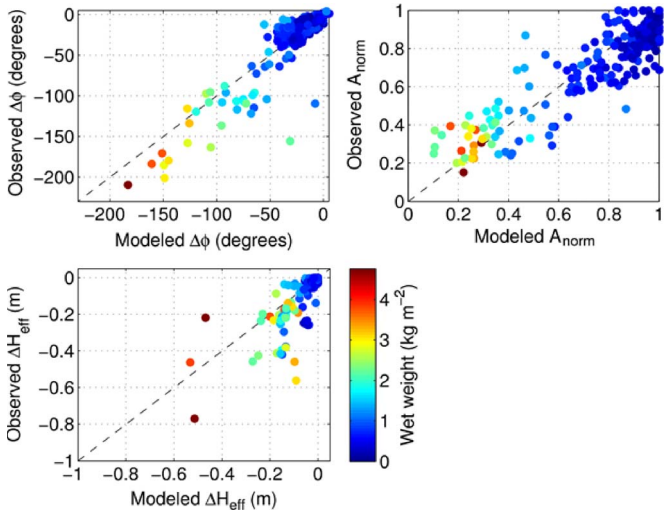


Fig. 6. Observed versus modeled SNR metrics, which includes data from all four field sites. Points are colored by the observed vegetation wet weight, which was used as model input. Observed metrics are the average, for a given day, of the metrics calculated using five satellite tracks. Modeled metrics are created using the average vegetation field parameters collected on that day. There is the same number of points in each panel. Many of the points in the $\Delta H_{\rm eff}$ plot are clustered around zero.

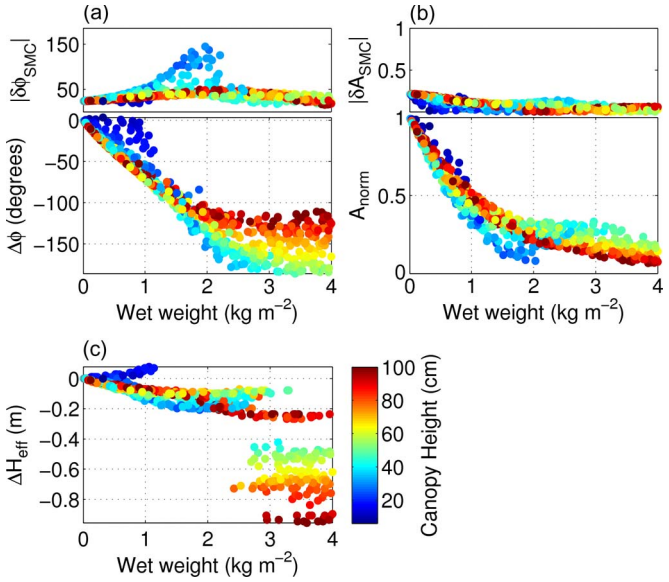


Fig. 7. Model SNR metrics using random combinations of vegetation parameters and a dry (0.05) soil moisture profile as input. Metrics are plotted against modeled vegetation wet weight and colored by modeled canopy height. (a) Absolute magnitude of phase change if a wet (0.40) soil moisture profile were used as input (top). The range of the box is the same as the range in the box below. The subscript SMC is used to denote that the phase change is from soil moisture only. (Bottom) Relationship between phase and vegetation wet weight for random model simulations with the dry soil moisture profile. (b) Absolute magnitude of normalized amplitude change if a wet (0.40) soil moisture profile were used as input (top). The range of the box is the same as the range in the box below. The subscript SMC is used to denote that the amplitude change is from soil moisture only. (Bottom) Relationship between normalized amplitude and vegetation wet weight for random model simulations with the dry soil moisture profile. (c) Relationship between change in effective reflector height and vegetation wet weight for random model simulations with the dry soil moisture profile.

each harvest. The return to preharvest values is not instantaneous, as the alfalfa is first cut and then left in the field for a period of a few days to dry before it is collected. Simulated metrics, based only on the average measured vegetation and soil moisture parameters, show the same variations associated with growth and harvest. The magnitude of change is the same as determined from the observed SNR data. The modeled SNR metric is always close to or falls within the mean $\pm$ standard deviation of the observed metric.

We now compare simulated and observed SNR metrics from all field sites in all years (Fig. 6). Modeled metrics were simulated using the average of measured vegetation parameters on each day and the average soil moisture value on the day during which vegetation was sampled. Observed metrics were calculated by averaging the SNR metrics from the five satellite tracks described previously. Simulated and observed $A_{\rm norm}$ values are highly correlated across the entire range of observed vegetation wet weight (0–5 kg $\cdot$ m$^{-2}$), with an $r^2$ value of 0.79 and root-mean-square error (rmse) of 0.12. The $r^2$ value between the modeled and observed values of $\Delta\phi$ is also very high (0.84), and the rmse is 20°. $H_{\rm eff}$ has the lowest $r^2$ of the three metrics, with a value of 0.62 and an rmse of 0.09 m. This is likely due to the fact that, when there is high vegetation, there are sometimes two very prominent reflector heights shown in the LSP, which compete to be the dominant frequency. Small adjustments in vegetation input would cause one reflector height to be slightly more powerful than the other, causing apparent jumps in $H_{\rm eff}$ time series.

## IV. How GPS Metrics Respond To Vegetation

We now describe how the simulated GPS metrics respond to changes in vegetation amount. We no longer use each field sample as model input, as was used for validation of the model. Instead, we use random combinations of vegetation parameters to create a library of model simulations. For these simulations, we allowed vegetation wet weight to vary between 0 and 4 kg $\cdot$ m$^{-2}$, canopy height between 1 and 100 cm, and vegetation percent water content (from which one can infer dry biomass) between 10% and 90%. However, we excluded parameter sets which resulted in permittivities higher than 1.1. This is much higher than the permittivity at the alfalfa site. Most GPS antennas that comprise the PBO network are located in environments with much lower biomass and vegetation water content than is found at the alfalfa site. Here, we did not assume a bulk density of vegetation. Instead, we set it directly proportional to its water content. Antenna height was set at 2.4 m, similar to most antennas in the PBO network. Our "dry" library included an underlying uniform soil moisture of 0.05. We also created an identical library of vegetation model simulations for "wet" conditions, in which we set soil moisture to 0.4. This allows us to investigate how changing soil moisture beneath a vegetation canopy will affect SNR metrics.

We computed $\Delta\phi$, $A_{\rm norm}$, and $H_{\rm eff}$ for each simulation, using satellite elevation angles 5°–30°. Metrics were zeroed or normalized as described previously, setting the baseline phase value to be the value for a dry bare soil. Fig. 7 (panels a and b (bottom) and c) shows how SNR metrics respond to changes in vegetation for our "dry" library (soil moisture $= 0.05$). Using

$\Delta H_{\text{eff}}$ as a proxy of vegetation change would not be a wise choice, as no simple relationship exists between this metric and vegetation. $\Delta\phi$ is a better option—a somewhat linear relationship exists between phase and vegetation wet weight up to about 1.5 kg $\cdot$ m$^{-2}$. $A_{\text{norm}}$ appears to also be a good proxy for vegetation change, as a linear relationship exists between the metric and vegetation wet weight for values $< 1.5$ kg $\cdot$ m$^{-2}$, and $A_{\text{norm}}$ is not as affected by changes in canopy height as phase is. The relationship is no longer linear past 1.5 kg $\cdot$ m$^{-2}$, but $A_{\text{norm}}$ could still be used to predict vegetation amount past this value. $A_{\text{norm}}$ monotonically decreases for vegetation wet weight up to 4.0 kg $\cdot$ m$^{-2}$, although the sensitivity does decrease at higher values.

How metrics will respond to vegetation types with different growth strategies is also shown. We can assume that different vegetation types will have different relationships between canopy height and wet weight throughout the growing season. The figure shows that a plant type that is relatively short but holds a lot of water will cause SNR metrics to respond very differently than a plant type that is tall with relatively little water. For example, a canopy with a wet weight of 4 kg $\cdot$ m$^{-2}$ could result in a phase decrease of between 110° and 175° from bare soil conditions, depending on whether the plants are short (relatively higher permittivity) or tall (relatively lower permittivity; Fig. 7(a), bottom).

Fig. 7(a) and (b) (top) indicates the change in phase or normalized amplitude if soil moisture changes from 0.05 to 0.4, for a given overlying vegetation canopy. Here, we have plotted the absolute value of the change and scaled each box to the range of their respective boxes below. We did not include the analogous panel for effective reflector height because changes exceeded $\pm$0.1 m, or 10% of the range, in only a handful of cases. Fig. 7(b) (top) shows that the influence of soil moisture on $A_{\text{norm}}$ is relatively small compared to the influence of vegetation on this metric. The figure also shows that the influence of soil moisture on normalized amplitude is relatively constant, compared to the $A_{\text{norm}}$ changes expected from vegetation. Thus, if one wanted to use $A_{\text{norm}}$ as a proxy for vegetation change, variations in soil moisture would only introduce small uncertainties. Fig. 7(a) (top) shows that the case for $\Delta\phi$ is different. The change in phase due to soil moisture is approximately one third of that caused by vegetation for most of the canopies that we tested. However, for short and dense canopies, $\Delta\phi$ from soil moisture is roughly equal to that from vegetation. This suggests that a large phase change could be due to either a change in soil moisture or in vegetation or concurrent changes in both.

The model simulates changes in both phase and amplitude from soil moisture across the range of canopies tested here. Intuitively, one would expect a decrease in sensitivity to soil moisture for denser vegetation canopies. This general effect is simulated by the model: The influence of soil moisture on phase does generally diminish as permittivity increases. However, the simulated vegetation canopy does not completely obscure soil moisture effects until the canopy permittivity exceeds $\sim$2.0 (not shown). The canopies tested here are primarily composed of air, so the permittivity is almost always between 1.01 and 1.10. These permittivity values are consistent with published values [35]. For these permittivity values, the vegetation canopy does not completely obscure the underlying soil. Thus, effects of varying soil moisture on phase must be considered.

Because reflection coefficients are dependent upon elevation angle and should be highest at grazing (low) angles, one might predict that certain elevation angles are more sensitive to changes in vegetation than others. We used the "dry" library model simulations to see whether restricting $A_{\text{norm}}$ analysis to 5°–15° would improve its relationship with vegetation wet weight. However, model results indicated that using 5°–15° would actually be worse in vegetation estimation, as the relationship between normalized amplitude and wet weight was less clear.

## V. Discussion

The electrodynamic model's ability to reproduce SNR data was shown in Section III. Comparisons between modeled and observed SNR metrics show that the model can successfully simulate changes in metrics for a variety of vegetated environments. Results from model simulations, presented in the previous section, show that both phase and amplitude vary roughly linearly with vegetation wet weight up to approximately 1.5 kg $\cdot$ m$^{-2}$ (Fig. 7). $A_{\text{norm}}$ continues to decrease with vegetation wet weight up to 4.0 kg $\cdot$ m$^{2}$, although the sensitivity to increasing vegetation amount decreases sharply beyond 1.5 kg $\cdot$ m$^{-2}$. Although the EM model can simulate these effects (Fig. 4), it is not possible to use a simple linear relationship to estimate changes in vegetation beyond 1.5 kg $\cdot$ m$^{-2}$. We now investigate why this is the case.

Once vegetation wet weight exceeds $\sim$1.5 kg $\cdot$ m$^{-2}$, $\Delta\phi$ is not a good indicator of vegetation amount. In addition, $A_{\text{norm}}$ is less sensitive to changes in vegetation amount above wet weight of $\sim$1.5 kg $\cdot$ m$^{-2}$. This is not necessarily because the SNR data themselves stop changing or saturate once vegetation exceeds this amount. The metrics, however, no longer describe the complex behavior of SNR data when there is a significant vegetation canopy present.

Equation (1), which has been in the past used to describe SNR data, was formulated under the assumption that there is one dominant frequency in the SNR data, either resulting from the soil surface or snow surface. However, in the presence of a vegetation layer, the power of the dominant frequency of the SNR data decreases [e.g., see Fig. 2(c)]. In extreme cases, there may be an equally dominant second frequency peak, indicating that the SNR data are actually comprised of two frequencies. In both of these cases, when the actual frequency of the SNR data does not match well with the frequency used to calculate phase and amplitude, errors will be introduced in the calculations. The constant phase and amplitude that are calculated may no longer be characteristic of the actual SNR data, if the data are comprised of multiple frequencies or have no dominant frequency. When the frequency discrepancy gets too large, which we posit is when wet weight exceeds 1.5 kg $\cdot$ m$^{-2}$, the errors in both phase and amplitude are too large to be representative of the changes occurring in SNR data. However, 1.5 kg $\cdot$ m$^{-2}$ should be used as a general guideline only, as plant types with different relationships between canopy

parameters may have a slightly higher or lower limit past which amplitude no longer varies nearly linearly with vegetation wet weight.

The difference between the frequency/*a priori* reflector height $(H_0)$ used to estimate phase and amplitude and the actual frequency(cies)/effective reflector height(s) $(H_{\text{eff}})$ of the SNR data is also responsible for the apparent increase in the response of phase to soil moisture for some vegetation canopies, which is seen in Fig. 7. There is nothing remarkable about certain vegetation canopies that would cause phase to respond more to soil moisture changes. To elucidate how the phase and soil moisture relationship changes when $H_0 - H_{\text{eff}}$ is large, we created multiple simulations of SNR data resulting from a bare soil, as was done in [19]. These simulations only differed in their surface soil moisture content, and profiles were uniform underneath the surface. We first calculated phase using the antenna height that we specified before running the model. This resulted in a phase to soil moisture relationship that is the same as is found in [19]. Next, we recalculated phase using a suite of antenna heights that were slightly higher or lower than the *a priori* height that was specified in the model. We found that the phase to soil moisture relationship changes depending on how large the discrepancy between the antenna height and the height used to estimate phase is. We believe that this is the reason why the relationship between phase and soil moisture responds unexpectedly once there is vegetation present.

## VI. Conclusion

The electrodynamic forward model used in this study has successfully simulated basic changes in GPS SNR data associated with vegetation canopies. The vegetation model has shown that, once vegetation canopy wet weight exceeds approximately 1.5 $\text{kg} \cdot \text{m}^{-2}$, as it would in some agricultural environments, the sensitivity of these metrics to changing vegetation decreases. Effective reflector height is never a consistent or reliable indicator of vegetation change. Using data from lower elevation angles, such as 5°–15°, does not improve the capability of amplitude to sense vegetation change when vegetation extent is high. When vegetation wet weight is below 1.5 $\text{kg} \cdot \text{m}^{-2}$, it could be possible to estimate wet weight using $\Delta\phi$ or $A_{\text{norm}}$ if surface soil moisture is known. When it is not known, $A_{\text{norm}}$ is the best metric to use to estimate vegetation wet weight.

A method that could quantify or include variation of frequency with elevation angle and the growth of vegetation would likely be more successful at describing changes in the vegetation canopy. The development of such a method or the use of an inverse procedure should be the subject of future efforts if we wish to successfully quantify high vegetation extent using SNR data.

## Acknowledgment

The authors would like to thank B. Hornbuckle of Iowa State University, T. Ochsner of Oklahoma State University, UNAVCO, and the reviewers for the helpful comments.

## References

[1] X. Zhang *et al.*, "Monitoring vegetation phenology using MODIS," *Remote Sens. Environ.*, vol. 84, no. 3, pp. 471–475, Mar. 2003.
[2] M. E. Brown, K. M. de Beurs, and M. Marshall, "Global phenological response to climate change in crop areas using satellite remote sensing of vegetation, humidity and temperature over 26 years," *Remote Sens. Environ.*, vol. 126, pp. 174–183, Nov. 2012.
[3] M. S. Moran, Y. Inoue, and E. M. Barnes, "Opportunities and limitations for image-based remote sensing in precision crop management," *Remote Sens. Environ.*, vol. 61, no. 3, pp. 319–346, Sep. 1997.
[4] T. Jackson, "Vegetation water content mapping using Landsat data derived normalized difference water index for corn and soybeans," *Remote Sens. Environ.*, vol. 92, no. 4, pp. 475–482, Sep. 2004.
[5] M. Pan *et al.*, "An initial assessment of SMOS derived soil moisture over the continental United States," *IEEE J. Sel. Topics Appl. Earth Observ. Remote Sens.*, vol. 5, no. 5, pp. 1448–1457, Oct. 2012.
[6] S. Gleason, S. Lowe, and V. Zavorotny, "Remote sensing using bistatic GNSS reflections," in *GNSS Applications and Methods*. Norwood, MA, USA: Artech House, 2009.
[7] A. Komjathy, V. U. Zavorotny, P. Axelrad, G. H. Born, and J. L. Garrison, "GPS signal scattering from sea surface: Wind speed retrieval using experimental data and theoretical model," *Remote Sens. Environ.*, vol. 73, no. 2, pp. 162–174, Aug. 2000.
[8] E. Cardellach *et al.*, "Mediterranean Balloon Experiment: Ocean wind speed sensing from the stratosphere, using GPS reflections," *Remote Sens. Environ.*, vol. 88, no. 3, pp. 351–362, Dec. 2003.
[9] S. Gleason *et al.*, "Detection and processing of bistatically reflected GPS signals from low Earth orbit for the purpose of ocean remote sensing," *IEEE Trans. Geosci. Remote Sens.*, vol. 43, no. 6, pp. 1229–1241, Jun. 2005.
[10] E. Cardellach, F. Fabra, A. Rius, S. Pettinato, and S. D'Addio, "Characterization of dry-snow sub-structure using GNSS reflected signals," *Remote Sens. Environ.*, vol. 124, pp. 122–134, Sep. 2012.
[11] N. Rodriguez-Alvarez *et al.*, "Snow monitoring using GNSS-R techniques," in *Proc. IEEE Int. Geosci. Remote Sens. Symp.*, 2011, pp. 4375–4378.
[12] N. Rodriguez-Alvarez *et al.*, "Vegetation water content estimation using GNSS measurements," *IEEE Geosci. Remote Sens. Lett.*, vol. 9, no. 2, pp. 282–286, Mar. 2012.
[13] N. Rodriguez-Alvarez *et al.*, "Review of crop growth and soil moisture monitoring from a ground-based instrument implementing the interference pattern GNSS-R technique," *Radio Sci.*, vol. 46, no. 6, pp. 1–11, Dec. 2011.
[14] E. E. Small, K. M. Larson, and J. J. Braun, "Sensing vegetation growth with reflected GPS signals," *Geophys. Res. Lett.*, vol. 37, no. 12, pp. 1–5, Jun. 2010.
[15] F. G. Nievinski and K. M. Larson, "Forward modeling of GPS multipath for near-surface reflectometry and positioning applications," *GPS Solutions*, vol. 18, no. 2, pp. 309–322, Jun. 2013.
[16] A. Egido *et al.*, "Global navigation satellite systems reflectometry as a remote sensing tool for agriculture," *Remote Sens.*, vol. 4, no. 12, pp. 2356–2372, Aug. 2012.
[17] K. M. Larson and F. G. Nievinski, "GPS snow sensing: Results from the EarthScope Plate Boundary Observatory," *GPS Solutions*, vol. 17, no. 1, pp. 41–52, Mar. 2012.
[18] K. M. Larson *et al.*, "Use of GPS receivers as a soil moisture network for water cycle studies," *Geophys. Res. Lett.*, vol. 35, no. 24, pp. 1–5, Dec. 2008.
[19] C. C. Chew, E. E. Small, K. M. Larson, and V. U. Zavorotny, "Effects of near-surface soil moisture on GPS SNR data: Development of a retrieval algorithm for soil moisture," *IEEE Trans. Geosci. Remote Sens.*, vol. 52, no. 1, pp. 537–543, Jan. 2014.
[20] K. M. Larson *et al.*, "GPS multipath and its relation to near-surface soil moisture content," *IEEE J. Sel. Topics Appl. Earth Obs. Remote Sens.*, vol. 3, no. 1, pp. 91–99, Mar. 2010.
[21] K. M. Larson, J. S. Löfgren, and R. Haas, "Coastal sea level measurements using a single geodetic GPS receiver," *Adv. Space Res.*, vol. 51, no. 8, pp. 1301–1310, Apr. 2013.
[22] K. M. Larson, R. D. Ray, F. G. Nievinski, and J. T. Freymueller, "The accidental tide gauge: A GPS reflection case study from Kachemak Bay, Alaska," *IEEE Geosci. Remote Sens. Lett.*, vol. 10, no. 5, pp. 1200–1204, Sep. 2013.
[23] W. H. Press, S. A. Teukolsky, W. T. Vetterline, and B. P. Flannery, *Numerical Recipes in Fortran 77*, 2nd ed. New York, NY, USA: Cambridge Univ. Press, 1992, pp. 569–573.
[24] P. Axelrad, K. M. Larson, and B. Jones, "Use of the correct satellite repeat period to characterize and reduce site-specific multipath errors," in *Proc. 18th Int. Tech. Meet. Satellite Division*, Sep. 2005, pp. 2638–2648, ION GNSS.

[25] V. U. Zavorotny *et al.*, "A physical model for GPS multipath caused by land reflections: Toward bare soil moisture retrievals," *IEEE J. Sel. Topics Appl. Earth Observ. Remote Sens.*, vol. 3, no. 1, pp. 1–11, Mar. 2010.
[26] M. T. Hallikainen, F. T. Ulaby, M. C. Dobson, M. A. El-Rayes, and L.-K. Wu, "Microwave dielectric behavior of wet soil—Part 1: Empirical models and experimental observations," *IEEE Trans. Geosci. Remote Sens.*, vol. GE-23, no. 1, pp. 25–34, Jan. 1985.
[27] K. Lee, R. Chawn Harlow, E. J. Burke, and W. J. Shuttleworth, "Application of a plane-stratified emission model to predict the effects of vegetation in passive microwave radiometry," *Hydrol. Earth Syst. Sci.*, vol. 6, no. 2, pp. 139–152, 2002.
[28] R. Bindlish and A. P. Barros, "Parameterization of vegetation backscatter in radar-based, soil moisture estimation," *Remote Sens. Environ.*, vol. 76, no. 1, pp. 130–137, Apr. 2001.
[29] T. Mo, B. J. Choudhury, T. J. Schmugge, J. R. Wang, and T. J. Jackson, "A model for microwave emission from vegetation-covered fields," *J. Geophys. Res.*, vol. 87, no. C13, pp. 11 229–11 237, Dec. 1982.
[30] M. Schwank, C. Mätzler, S. Member, M. Guglielmetti, and H. Flühler, "L-band radiometer measurements of soil water under growing clover grass," *IEEE Trans. Geosci. Remote Sens.*, vol. 43, no. 10, pp. 2225–2237, Oct. 2005.
[31] F. T. Ulaby and E. A. Wilson, "Microwave attenuation properties of vegetation canopies," *IEEE Trans. Geosci. Remote Sens.*, vol. GE-23, no. 5, pp. 746–753, Sep. 1985.
[32] F. T. Ulaby and M. A. El-Rayes, "Microwave dielectric spectrum of vegetation—Part II: Dual-dispersion model," *IEEE Trans. Geosci. Remote Sens.*, vol. GE-25, no. 5, pp. 550–557, Sep. 1987.
[33] S. O. Nelson, "Dielectric properties of agricultural products—Measurements and applications," *IEEE Trans. Instrum. Meas.*, vol. 26, no. 5, pp. 845–869, Oct. 1991.
[34] E. P. W. Attema and F. T. Ulaby, "Vegetation modeled as a water cloud," *Radio Sci.*, vol. 13, no. 2, pp. 357–364, Mar. 1978.
[35] E. J. Burke, R. C. Harlow, and T. P. A. Ferré, "Measuring the dielectric permittivity of a plant canopy and its response to changes in plant water status: An application of impulse time domain transmission," *Plant Soil*, vol. 268, no. 1, pp. 123–133, Jan. 2005.
[36] K. M. Larson *et al.*, "Using GPS multipath to measure soil moisture fluctuations: Initial results," *GPS Solutions*, vol. 12, no. 3, pp. 173–177, Aug. 2008.
[37] W. Wan, K. M. Larson, E. E. Small, C. C. Chew, and J. J. Braun, "Using geodetic GPS receivers to measure vegetation water content," in *Proc. GPS Solutions*, May 2014, pp. 1–12.

**Clara C. Chew** received the B.A. degree in environmental studies from Dartmouth College, Hanover, NH, USA, in 2009. She is currently working toward the Ph.D. degree in geological sciences in the Department of Geological Sciences, University of Colorado, Boulder, CO, USA.

Her research interests include surface hydrology and remote sensing.

**Eric E. Small** received the B.A. degree in geological sciences from Williams College, Williamstown, MA, USA, in 1993 and the Ph.D. degree in earth sciences from the University of California, Santa Cruz, CA, USA, in 1998.

He is a Professor with the Department of Geological Sciences, University of Colorado, Boulder, CO, USA. His research is focused on land surface hydrology.

**Kristine M. Larson** received the B.A. degree in engineering sciences from Harvard University, Cambridge, MA, USA, in 1985 and the Ph.D. degree in geophysics from the Scripps Institution of Oceanography, University of California at San Diego, La Jolla, CA, USA, in 1990.

From 1988 to 1990, she was a Member of the Technical Staff at the Jet Propulsion Laboratory, California Institute of Technology, Pasadena, CA. Since 1990, she has been a Professor with the Department of Aerospace Engineering Sciences, University of Colorado, Boulder, CO, USA. Her research interests focus on developing new applications and techniques for GPS.

**Valery U. Zavorotny** (M'01–SM'03–F'10) received the M.Sc. degree in radio physics from Gorky State University, Gorky, Russia, in 1971 and the Ph.D. degree in physics and mathematics from the Institute of Atmospheric Physics, Union of Soviet Socialist Republics Academy of Sciences, Moscow, Russia, in 1979.

From 1971 to 1990, he was a Research Scientist with the Institute of Atmospheric Physics, USSR Academy of Sciences. In 1990, he joined Lebedev Physical Institute, Moscow. From 1991 to 2000, he was a Cooperative Institute for Research in Environmental Sciences Research Associate with the Environmental Technology Laboratory (currently called Earth Systems Research Laboratory together with five other laboratories), National Oceanic and Atmospheric Administration, Boulder, CO, USA, where he became a Physicist in 2000. His research interests include theory of wave propagation through random media, wave scattering from rough surfaces, and ocean and land remote sensing applications.

Dr. Zavorotny is a member of Commission F of the U.S. National Committee of URSI and the American Geophysical Union.